J. Fluid Mech. (2018), *vol.* 836, *pp.* 998–1008.
doi:10.1017/jfm.2017.839

On the hydrodynamic and acoustic nature of pressure proper orthogonal decomposition modes in the near field of a compressible jet

Matteo Mancinelli[1],†, Tiziano Pagliaroli[2], Roberto Camussi[1] and Thomas Castelain[3]

[1]Dipartimento di Ingegneria, Università degli Studi Roma Tre, Via della Vasca Navale 79, 00146 Rome, Italy

[2]Dipartimento di Ingegneria, Università degli Studi Niccolò Cusano, Via Don Carlo Gnocchi 3, 00166 Rome, Italy

[3]Laboratoire de Mécanique des Fluides et d'Acoustique – UMR 5509, École Centrale de Lyon, 36 av. Guy de Collongue, 69134 Ecully CEDEX, France

(Received 10 July 2017; revised 6 October 2017; accepted 14 November 2017)

In this work an experimental investigation of the near-field pressure of a compressible jet is presented. The proper orthogonal decomposition (POD) of the pressure fluctuations measured by a linear array of microphones is performed in order to provide the streamwise evolution of the jet structure. The wavenumber–frequency spectrum of the space–time pressure fields re-constructed using each POD mode is computed in order to provide the physical interpretation of the mode in terms of hydrodynamic/acoustic nature. Specifically, non-radiating hydrodynamic, radiating acoustic and 'hybrid' hydro-acoustic modes are found based on the phase velocity associated with the spectral energy bumps in the wavenumber–frequency domain. Furthermore, the propagation direction in the far field of the radiating POD modes is detected through the cross-correlation with the measured far-field noise. Modes associated with noise emissions from large/fine scale turbulent structures radiating in the downstream/sideline direction in the far field are thus identified.

Key words: aeroacoustics, jet noise

1. Introduction

Despite many years of research activity, the mechanism by which the turbulent structures in the jet generate noise is still a matter for debate. Since the seminal work of Lighthill (1952), significant progress has been made in terms of the understanding and modelling of jet noise (see e.g. Lilley 1991; Tam, Golebiowski & Seiner 1996; Cavalieri *et al.* 2011 and Jordan & Colonius 2013). Nevertheless, all the pieces of the puzzle have not yet been collected and further efforts are needed to have a clear picture of the jet noise production and propagation mechanisms.

† Email address for correspondence: matteo.mancinelli@uniroma3.it

Indeed, the investigation of the near region of the jet is essential to improve the knowledge of the jet physics and to identify the acoustic sources with the aim of developing noise control devices. As pointed out by Bonnet *et al.* (1994), the use of the proper orthogonal decomposition is a powerful tool to clarify the organised motion of the jet. To this extent, the POD was applied by Arndt, Long & Glauser (1997) to pressure fluctuations measured in the near field in order to deduce the streamwise structure of the jet, the eigenfunctions being characterised by the amplification–saturation–decay trend of an instability wave. Nevertheless, the mere existence of POD modes does not imply that they have dynamical significance, especially in terms of noise generation (Freund & Colonius 2009). Indeed, the near-field energetic structures deduced by the POD are not necessarily representative of the noise-generating flow. This point was addressed by Picard & Delville (2000), who exploited the linear stochastic estimation to interpret the near-field pressure POD modes in terms of velocity field for the computation of the far-field noise. Nevertheless, an acoustical identification of the coherent flow structure educed by the POD is still far from being reached.

The discussion above motivated this work, whose main novelty lies in the presentation of a physical criterion for the interpretation of the near-field pressure POD modes in the streamwise direction in terms of hydrodynamic and acoustic pressures. Indeed, a microphone in the near field senses the fluctuations related to the non-radiating hydrodynamic pressure and the perturbations associated with the propagating acoustic pressure (Howes 1960). The necessity of separating the pseudo-sound and sound components led to the development of different approaches (see Arndt *et al.* 1997; Tinney & Jordan 2008; Grizzi & Camussi 2012 and the recent papers by Mancinelli *et al.* 2016, 2017*b*). In this work the hydrodynamic or acoustic nature of the POD modes is assessed through the computation of the wavenumber–frequency spectrum of the near pressure field re-constructed using each POD mode. Specifically, on account of the phase velocity of the associated spectral energy bumps in the k_x–ω domain, hydrodynamic, acoustic and 'hybrid' hydro-acoustic modes are detected for the first time. The propagation direction of the acoustic and hydro-acoustic radiating modes is identified through the correlation with the measured far-field noise. The analysis reveals a deeper overview of the sound generation and provides a range of k_x and ω to be manipulated by control devices in order to reduce the acoustic emissions, the application of closed-loop control systems to experimental data being still a challenging task for the future, as recently pointed out by Sasaki *et al.* (2017).

The paper is organised as follows. In § 2 a brief description of the experiment is given, whereas § 3 is devoted to the proper orthogonal decomposition of the near pressure field. The identification of the hydrodynamic, acoustic and hybrid modes through the wavenumber–frequency spectrum is presented in § 4. Conclusions are addressed in § 5.

2. Experimental set-up

Experiments were carried out in the anechoic wind tunnel in the Centre Acoustique of Laboratoire de Mécanique des Fluides et d'Acoustique at the École Centrale de Lyon. Simultaneous near- and far-field pressure measurements were performed on a single-stream jet for Mach numbers $M_j = 0.6$ and 0.9, to which correspond nozzle diameter-based Reynolds numbers of 7.5×10^5 and 1.2×10^6, respectively. The 14-microphone array in the near field was placed in the so-called linear hydrodynamic

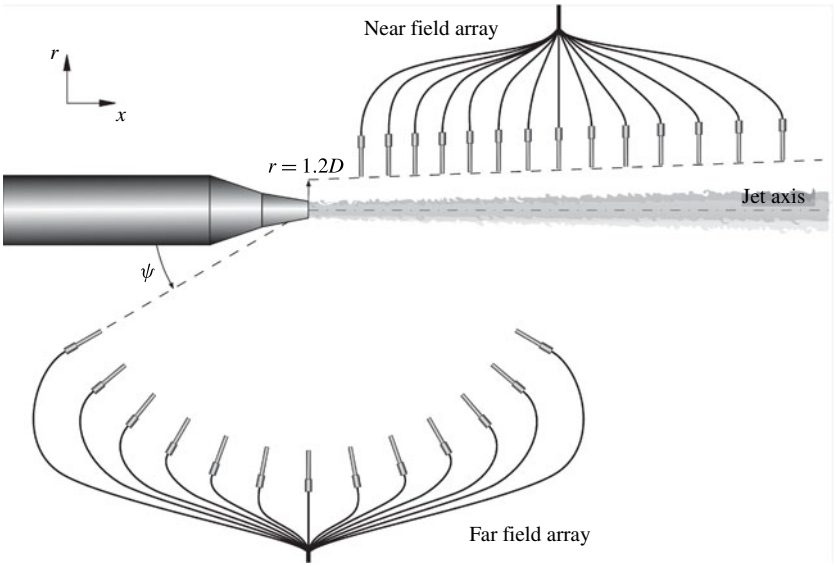

FIGURE 1. Sketch of the experimental set-up and microphones disposition.

regime (Suzuki & Colonius 2006) on a line following the jet spreading angle, the intercept of this line with the nozzle exit plane being at a radial distance $r/D = 1.2$ from the jet axis. The microphones locations in the streamwise direction spanned an axial distance range $x/D = [2, 8.7]$. The 13-microphone array in the far field was located on a circular arc at a radial distance $r/D = 40$ from the nozzle exhaust spanning a polar angle range $\psi = [30°, 150°]$, the polar angle being defined positive in the upstream direction. A sketch of the experimental set-up as well as a scheme of the microphones disposition is shown in figure 1.

The pressure fluctuations induced by the jet were measured by PCB 377B01 microphones. Time signals were acquired by National Instruments PXI-4472 system with a sampling frequency of 51.2 kHz for an acquisition time of 10 s. A preliminary test campaign was carried out to assess the accuracy of the experimental data. The acquisition parameters were carefully chosen in order to have an interval confidence of 99 % with a maximum uncertainty of 2 % for the evaluation of the statistical moments of interest, i.e. up to the fourth order (Tropea, Yarin & Foss 2007; Mancinelli, Di Marco & Camussi 2017*a*).

For a more detailed description of the experimental set-up and a qualification of the jet facility the reader may refer to Mancinelli *et al.* (2017*b*).

3. Proper orthogonal decomposition of the near pressure field

For a comprehensive review on mathematical aspects of proper orthogonal decomposition and its application to turbulent flows the reader may refer to the large body of literature (e.g. Berkooz, Holmes & Lumley 1993). In this work the POD is applied to the near pressure field $p(x, t)$ in the streamwise direction x as in Arndt *et al.* (1997) and Picard & Delville (2000). The Fredholm integral eigenvalue problem reduces to the following:

$$\int_{D_x} R(x, x')\Phi_n(x')\,\mathrm{d}x' = \lambda_n(x)\Phi_n(x), \tag{3.1}$$

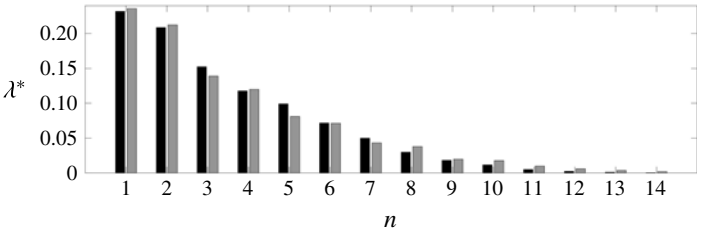

FIGURE 2. Normalised eigenvalues for both jet Mach numbers: black bars refer to $M_j = 0.6$, grey bars to $M_j = 0.9$.

where $R(x, x')$ is the auto-covariance matrix of the pressure field, $\Phi_n(x)$ and $\lambda_n(x)$ are the eigenfunctions and eigenvalues, respectively. It has to be underlined that $N = 14$ modes are obtained for the present case, being 14 the number of microphones of the near-field array. The approximated space–time pressure field $\tilde{p}(x, t)$ can be recovered by summing all the POD modes, as reported in the following:

$$\tilde{p}(x, t) = \sum_{n=1}^{N} \tilde{p}_n(x, t) = \sum_{n=1}^{N} a_n(t)\Phi_n(x), \tag{3.2}$$

where $a_n(t)$ are the projection coefficients of the near pressure field over the eigenfunctions, as formally defined in the following:

$$a_n(t) = \int_{D_x} p(x, t)\Phi_n(x)\,\mathrm{d}x. \tag{3.3}$$

In reference to (3.2), it has to be pointed out that the mean pressure is zero since the microphones measure only the fluctuating pressure.

Figure 2 shows the normalised eigenvalues λ^* for both jet Mach numbers, the normalisation being achieved by dividing each eigenvalue by the sum of all the eigenvalues. As outlined by Arndt *et al.* (1997), the eigenvalues provide an estimation of the coherent energy embedded in each POD mode. It is observed that the eigenvalue spectrum is almost independent of the jet Mach number and that the energy is distributed on a wide range of modes showing an exponential-like decay. The evolution along the streamwise direction of the first two POD modes, that are the most energetic ones, is represented in figure 3 for both M_j. The trend is qualitatively in agreement with the typical instability wave shape reported by Arndt *et al.* (1997) and Picard & Delville (2000). As for the eigenvalues, no significant effect of the jet Mach number can be detected.

The space–time map of the original near pressure field and the re-constructed pressure fields using each POD mode is shown in figure 4. For the sake of brevity, the case $M_j = 0.6$ was considered here as well as the first 8 POD modes for the re-construction of the space–time pressure fields. The re-constructed pressure fields show an organised structure, that is a chessboard-like pattern with characteristic wavelengths and time scales strongly dependent on the POD mode considered. It has to be pointed out that the characteristic wavelengths appear to change with the streamwise position, the resulting pattern being non-uniform in space.

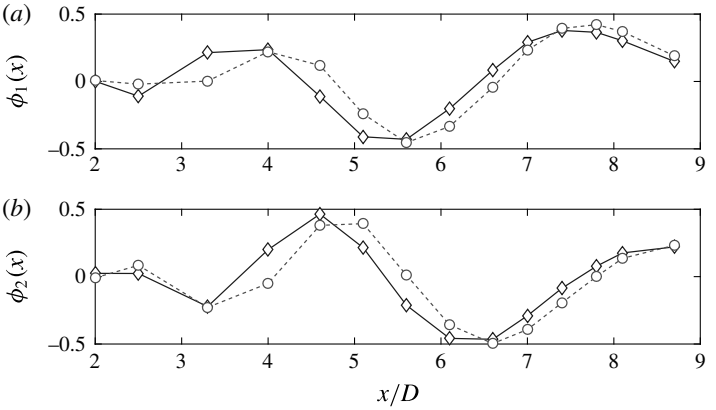

FIGURE 3. Trend of the first two POD modes along the streamwise direction for both jet Mach numbers: ◇ refer to $M_j = 0.6$, ○ to $M_j = 0.9$. (*a*) First POD mode, (*b*) second POD mode.

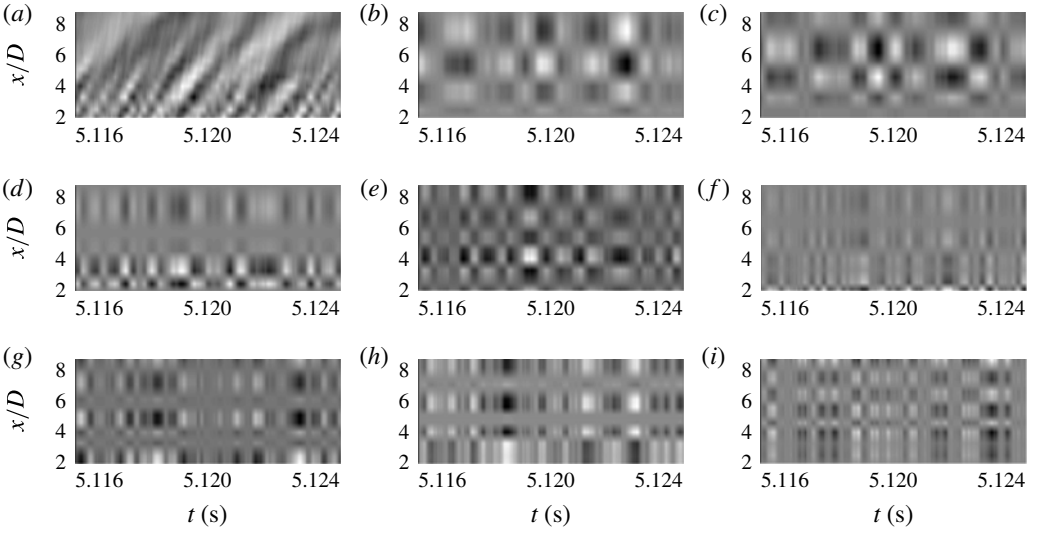

FIGURE 4. Space–time map of the original near pressure field $p(x, t)$ and the re-constructed pressure fields $\tilde{p}_n(x, t)$ using each POD mode for jet Mach number $M_j = 0.6$. (*a*) $p(x, t)$, (*b*) $\tilde{p}_1(x, t)$, (*c*) $\tilde{p}_2(x, t)$, (*d*) $\tilde{p}_3(x, t)$, (*e*) $\tilde{p}_4(x, t)$, (*f*) $\tilde{p}_5(x, t)$, (*g*) $\tilde{p}_6(x, t)$, (*h*) $\tilde{p}_7(x, t)$, (*i*) $\tilde{p}_8(x, t)$.

4. Identification of hydrodynamic, acoustic and hybrid modes

The chessboard-like pattern of the re-constructed pressure fields with different wavelengths and time scales suggests that the energy content of the associated wavenumber–frequency spectrum should be concentrated on a well-defined k_x–ω region. The hydrodynamic or acoustic nature of the re-constructed $\tilde{p}_n(x, t)$, and hence of the associated POD modes, can be assessed based on the location of the spectral energy in the k_x–ω domain and on account of its phase velocity. According to Tinney & Jordan (2008), POD modes generating pressure fields characterised by a spectral

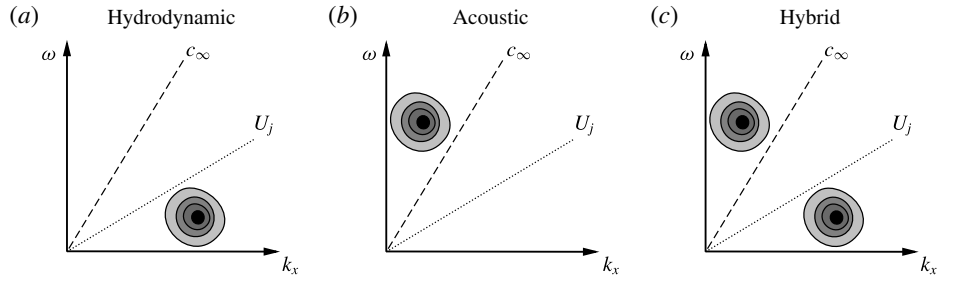

FIGURE 5. Scheme of interpretation of the POD modes based on the location of the spectral energy in the k_x–ω domain: (*a*) hydrodynamic, (*b*) acoustic, (*c*) hydro-acoustic or hybrid.

POD modes identification		
Mode type	$M_j = 0.6$	$M_j = 0.9$
Hydrodynamic	1, 2, 4, 7, [10, 14]	1, 2, 3, 7, 8
Acoustic	9	9, 12, 13, 14
Hybrid 1	3	4
Hybrid 2	5, 6	5, 6, 10, 11
Hybrid 3	8	—

TABLE 1. Summary of the types of POD modes detected based on the phase velocity of the k_x–ω spectrum of the re-constructed $\tilde{p}_n(x, t)$ for both jet Mach numbers.

energy bump with a phase velocity lower than the ambient speed of sound and of the order of the jet velocity are identified as hydrodynamic. On the other hand, POD modes providing re-constructed pressure fields with a phase velocity greater than or equal to the speed of sound are identified as acoustic. The re-constructed pressure fields whose wavenumber–frequency spectrum exhibit several energy bumps in the k_x–ω domain having phase velocities greater and lower than the speed of sound are associated with hydro-acoustic or 'hybrid' modes. A schematic representation of the identification process reported above is depicted in figure 5.

Three types of hybrid modes were detected. The mode denoted as hybrid 1 presented four spectral energy bumps, one of them having a phase velocity of the order of the speed of sound. On the contrary, the modes denoted as hybrid 2 and 3 presented two energy bumps, one bump having a phase velocity greater than or equal to the speed of sound.

On account of the topology of the k_x–ω spectrum, the nature of each POD mode for both M_j is summarised in table 1. The mode topology is analogous for both M_j, with the exception of the hybrid 3 mode, this type of mode being detected only for $M_j = 0.6$. It has to be pointed out that the identification of the mode type does not have the same numbering order between the two M_j, the numbering order being dependent on the energy of each mode. As expected, the first POD modes, that are the most energetic ones, exhibit a hydrodynamic nature. It is interesting to underline that the number of the acoustic modes is larger for $M_j = 0.9$, this result being related to the higher sensitiveness of the acoustic pressure to the jet Mach number variation (Mancinelli *et al.* 2017*b*).

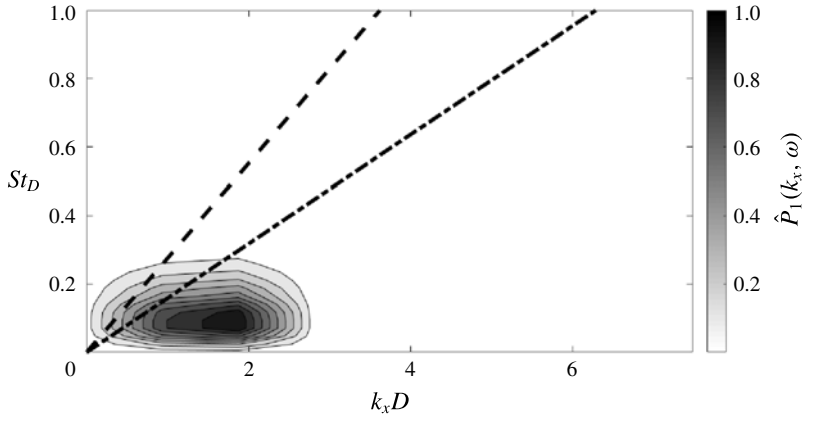

FIGURE 6. Wavenumber–frequency spectrum of $\tilde{p}_1(x, t)$ for $M_j = 0.6$, whose associated POD mode is identified as hydrodynamic. Dashed line refers to the speed of sound, dash-dotted line to the jet velocity.

The wavenumber–frequency spectrum of the re-constructed pressure fields are reported in the following. Each type of mode described above is presented and physically interpreted. The two-dimensional (2-D) Fourier transform of the space–time pressure fields is computed as follows:

$$\hat{p}_n(k_x, \omega) = \int_{-\infty}^{+\infty} \int_{-\infty}^{+\infty} \tilde{p}_n(x, t) W(x) W(t) \mathrm{e}^{-\mathrm{i}(k_x x + \omega t)} \, \mathrm{d}x \, \mathrm{d}t, \tag{4.1}$$

where $W(x)$ and $W(t)$ are Hamming windowing functions in the space and time domains, respectively. The wavenumber–frequency spectrum is given by the following:

$$\hat{P}_n(k_x, \omega) = \hat{p}_n(k_x, \omega) \hat{p}_n^*(k_x, \omega). \tag{4.2}$$

The 2-D spectra are presented in dimensionless form, the normalisation being achieved by dividing the spectrum by the spectral energy peak. Furthermore, the frequencies are reported in terms of Strouhal number based on the nozzle diameter and the jet velocity, whereas the wavenumber is normalised by multiplying by the nozzle diameter.

Figure 6 shows the k_x–ω spectrum of a hydrodynamic mode. As an example the re-constructed $\tilde{p}_1(x, t)$ for $M_j = 0.6$ was considered here. Only positive wavenumbers and frequencies are shown, the spectrum being symmetric with respect to the origin. As expected, the energy content is concentrated on a well-defined k_x–ω band. Specifically, the spectral energy bump has a characteristic phase velocity lower than the jet velocity, the associated POD mode being identified as hydrodynamic.

Figure 7(*a*) shows the k_x–ω spectrum of $\tilde{p}_9(x, t)$ for $M_j = 0.9$. For the sake of clarity of the representation both negative and positive wavenumbers and frequencies are reported. It is observed that the spectral energy bump is characterised by a phase velocity that is much larger than the speed of sound, this feature suggesting the acoustic nature of the associated POD mode. It is interesting to point out that the associated phase velocity tends to infinity, thus indicating acoustic waves propagating orthogonal to the near-field microphone array axis and hence in the sideline direction in the far field. Such assertion is further supported by computing the cross-correlation

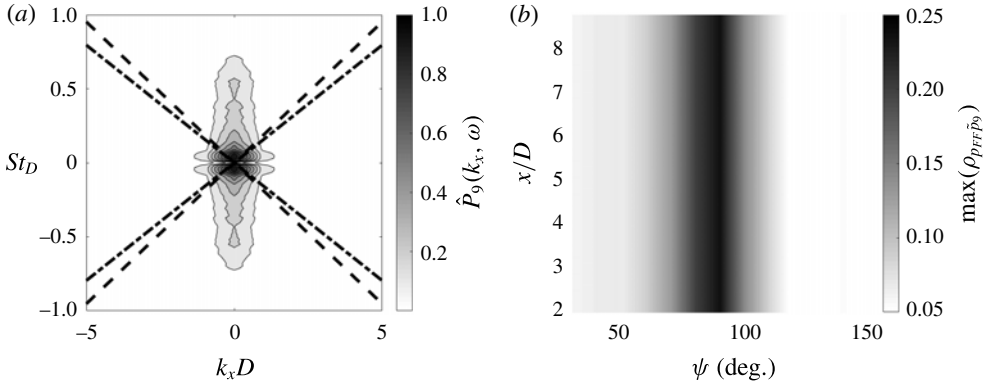

FIGURE 7. (*a*) Wavenumber–frequency spectrum of $\tilde{p}_9(x, t)$ for $M_j = 0.9$, whose associated POD mode is identified as acoustic. Dashed lines refer to the speed of sound, dash-dotted lines to the jet velocity. (*b*) Cross-correlation coefficient peak map between far-field pressure and re-constructed $\tilde{p}_9(x, t)$ for $M_j = 0.9$ at all the axial and polar positions.

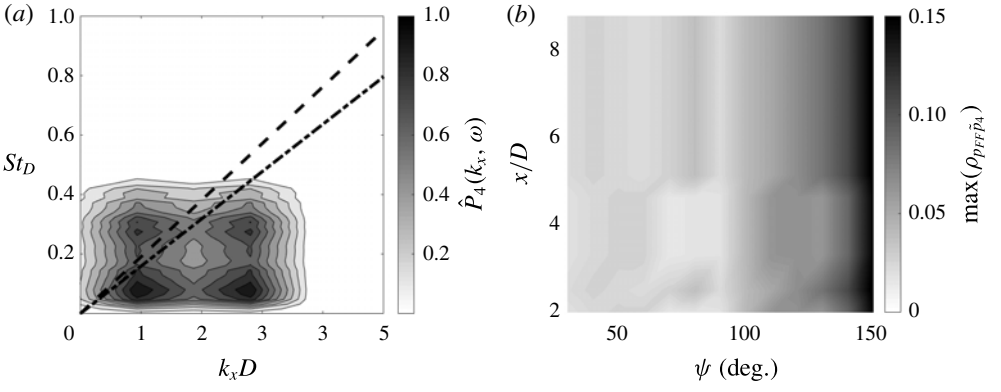

FIGURE 8. (*a*) Wavenumber–frequency spectrum of $\tilde{p}_4(x, t)$ for $M_j = 0.9$, whose associated POD mode is identified as hybrid 1. Dashed line refers to the speed of sound, dash-dotted line to the jet velocity. (*b*) Cross-correlation coefficient peak map between far-field pressure and re-constructed $\tilde{p}_4(x, t)$ for $M_j = 0.9$ at all the axial and polar positions.

between the far-field pressure and the re-constructed near-field pressure. Figure 7(*b*) shows the contour map of the cross-correlation coefficient peaks for all the near-field streamwise positions and all the far-field polar positions. It is observed that large correlation values are detected for all the axial positions only for polar angles in the neighbourhood of $\psi = 90°$ in the far field, thus confirming the preferential propagation direction in the sideline.

The wavenumber–frequency spectrum of the re-constructed $\tilde{p}_4(x, t)$ for $M_j = 0.9$ is represented in figure 8(*a*), the associated POD mode being of the hybrid 1 type. Four main energy bumps are detected, one of them having a phase velocity of the order of the speed of sound. Such a behaviour implies the presence of acoustic waves travelling parallel to the near-field array axis and thus suggesting a downstream preferential propagation direction in the far field. The cross-correlation coefficient peak map between the far-field noise and the re-constructed $\tilde{p}_4(x, t)$ was computed

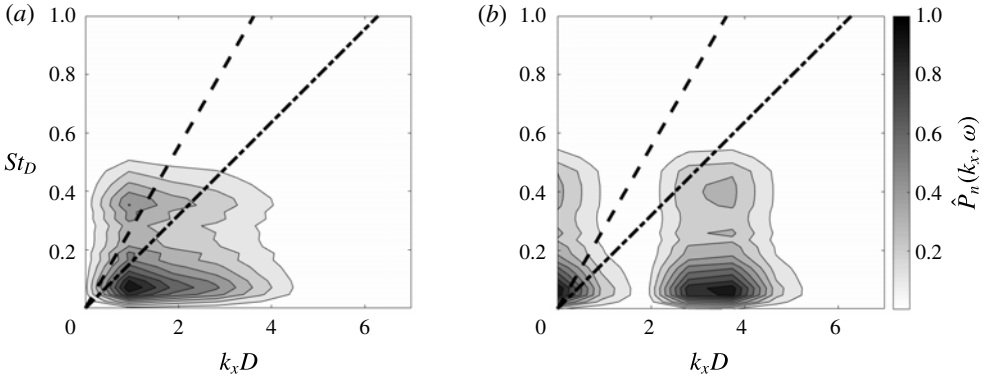

FIGURE 9. Wavenumber–frequency spectrum for $M_j = 0.6$: (*a*) $\tilde{p}_6(x, t)$, whose associated POD mode is identified as hybrid 2; (*b*) $\tilde{p}_8(x, t)$, whose associated POD mode is identified as hybrid 3. Dashed line refers to the speed of sound, dash-dotted line to the jet velocity.

for all x/D and ψ, its representation being reported in figure 8(*b*). It is clear that larger correlation levels are found for increasing polar angles, thus confirming the preferential radiation in the aft arc.

The k_x–ω spectra of $\tilde{p}_6(x, t)$ and $\tilde{p}_8(x, t)$ for $M_j = 0.6$ are shown in figure 9, the associated POD modes being of hybrid 2 and 3 types, respectively. The hybrid 2 mode is characterised by two energy bumps at the same wavenumber but different frequency, one bump having a phase velocity close to the speed of sound and being related to acoustic perturbations propagating in the downstream direction. The hybrid 3 mode exhibits two main bumps at the same f with a different k_x, the associated acoustic content having a phase velocity tending to infinity and hence being related to acoustic waves radiating in the sideline direction.

5. Conclusions

In this paper the proper orthogonal decomposition of the near pressure field in the streamwise direction was performed. The POD modes have been interpreted in terms of their hydrodynamic or acoustic nature through the computation of the wavenumber–frequency spectrum of the re-constructed space–time pressure fields using each POD mode. The identification of the nature of the modes was achieved on account of the localisation in the k_x–ω domain of the spectral energy bump through the comparison of its characteristic phase velocity with the ambient speed of sound. To the best of the authors' knowledge, this represents the first attempt to provide a criterion for the physical interpretation and for the attribution of dynamical significance of the pressure POD modes in terms of representativeness of the noise generating flow.

The analysis of the topology of the k_x–ω spectrum of each re-constructed pressure field revealed the presence of three classes of modes: hydrodynamic, acoustic and hydro-acoustic or hybrid. The hydrodynamic and acoustic modes were characterised by a spectral energy bump with a phase velocity of the order of the jet velocity and greater than or equal to the ambient speed of sound, respectively. The hybrid modes exhibited several energy bumps with different phase velocities. Three types of hybrid modes were detected based on the topology of the wavenumber–frequency spectrum. The propagation direction in the far field of the radiating acoustic content of the POD modes was investigated establishing a causality relation through the computation of the

cross-correlation with the measured far-field noise. Specifically, modes associated with noise emissions radiating in the downstream/sideline direction, i.e. related to sound emissions from large/fine scale turbulent structures, were identified for the first time.

Future developments of the present work will involve a better definition of the role of the hybrid modes in the jet noise production in order to shed light on the link between the noise-generating hydrodynamic turbulent structures and the resulting acoustic perturbations. This result could be achieved by a band-pass filtering of the hydrodynamic and acoustic components embedded in the hybrid modes in order to establish a coupling or causality relation between the two pressure components. Such an application could permit to identify a trace of the noise generation mechanism highlighting the characteristic wavelengths and time scales of the flow structures associated with the acoustic emissions. This point is essential to implement passive or active noise control strategies having an effect on the energy content in the k_x–ω band more efficient in terms of noise emissions.

Finally, it is authors' opinion that the new approach presented herein can represent a framework for several further research activities in the field of physical understanding of jet noise, reduced-order modelling of jet flow dynamics and noise control.

Acknowledgements

The authors acknowledge the support of the EU Collaborative project ORINOCO (ACP0-GA-2010-266103). M.M. and R.C. also acknowledge the partial support of the EU Collaborative project JERONIMO (ACP2-GA-2012-314692). Both the projects are funded under the 7th Framework Programme.

REFERENCES

ARNDT, R. E. A., LONG, D. F. & GLAUSER, M. N. 1997 The proper orthogonal decomposition of pressure fluctuations surrounding a turbulent jet. *J. Fluid Mech.* **340**, 1–33.

BERKOOZ, G., HOLMES, P. & LUMLEY, J. L. 1993 The proper orthogonal decomposition in the analysis of turbulent flows. *Annu. Rev. Fluid Mech.* **25** (1), 539–575.

BONNET, J. P., COLE, D. R., DELVILLE, J., GLAUSER, M. N. & UKEILEY, L. S. 1994 Stochastic estimation and proper orthogonal decomposition: complementary techniques for identifying structure. *Exp. Fluids* **17** (5), 307–314.

CAVALIERI, A. V. G., JORDAN, P., AGARWAL, A. & GERVAIS, Y. 2011 Jittering wave-packet models for subsonic jet noise. *J. Sound Vib.* **330** (18), 4474–4492.

FREUND, J. B. & COLONIUS, T. 2009 Turbulence and sound-field POD analysis of a turbulent jet. *Intl J. Aeroacoust.* **8** (4), 337–354.

GRIZZI, S. & CAMUSSI, R. 2012 Wavelet analysis of near-field pressure fluctuations generated by a subsonic jet. *J. Fluid Mech.* **698**, 93–124.

HOWES, W. L. 1960 Distribution of time-averaged pressure fluctuations along the boundary of a round subsonic jet. *Technical Report* NASA-TN-D-468. NASA.

JORDAN, P. & COLONIUS, T. 2013 Wave packets and turbulent jet noise. *Annu. Rev. Fluid Mech.* **45**, 173–195.

LIGHTHILL, M. J. 1952 On sound generated aerodynamically I. General theory. *Proc. R. Soc. Lond.* A **211** (1107), 564–587.

LILLEY, G. M. 1991 Jet noise classical theory and experiments. *Aeroacoust. Flight Vehicles* **1**, 211–289.

MANCINELLI, M., DI MARCO, A. & CAMUSSI, R. 2017*a* Multi-variate and conditioned statistics of velocity and wall pressure fluctuations induced by a jet interacting with a flat-plate. *J. Fluid Mech.* **823**, 134–165.

MANCINELLI, M., PAGLIAROLI, T., DI MARCO, A., CAMUSSI, R. & CASTELAIN, T. 2017*b* Wavelet decomposition of hydrodynamic and acoustic pressures in the near field of the jet. *J. Fluid Mech.* **813**, 716–749.

MANCINELLI, M., PAGLIAROLI, T., DI MARCO, A., CAMUSSI, R., CASTELAIN, T. & LÉON, O. 2016 Hydrodynamic and acoustic wavelet-based separation of the near-field pressure of a compressible jet. In *22nd AIAA/CEAS Aeroacoustics Conference*, *AIAA Paper* 2016-2864. American Institute of Aeronautics and Astronautics.

PICARD, C. & DELVILLE, J. 2000 Pressure velocity coupling in a subsonic round jet. *Intl J. Heat Fluid Flow* **21** (3), 359–364.

SASAKI, K., CAVALIERI, A. V. G., SILVESTRE, F. J., JORDAN, P., TISSOT, G. & BIAU, D. 2017 A framework for closed-loop flow control using the parabolized stability equations. In *23rd AIAA/CEAS Aeroacoustics Conference*, *AIAA Paper* 2017-3003. American Institute of Aeronautics and Astronautics.

SUZUKI, T. & COLONIUS, T. 2006 Instability waves in a subsonic round jet detected using a near-field phased microphone array. *J. Fluid Mech.* **565**, 197–226.

TAM, C. K. W., GOLEBIOWSKI, M. & SEINER, J. M. 1996 On the two components of turbulent mixing noise from supersonic jets. In *2nd AIAA/CEAS Aeroacoustics Conference*, *AIAA Paper* 1996-1716. American Institute of Aeronautics and Astronautics.

TINNEY, C. E. & JORDAN, P. 2008 The near pressure field of co-axial subsonic jets. *J. Fluid Mech.* **611**, 175–204.

TROPEA, C., YARIN, A. L. & FOSS, J. F. (Eds) 2007 *Springer Handbook of Experimental Fluid Mechanics*, vol. 23. Springer Science & Business Media.